https://doi.org/10.3311/PPci.20491

Periodica Polytechnica Civil Engineering, 67(1), pp. 123–140, 2023

Mechanical Behavior of Soil Foundations Reinforced with Geosynthetics Exposed to Normal and Reverse Fault Ruptures

Nabiollah Ahmadi[1], Meysam Fadaee[1*]

[1] Department of Civil Engineering, Science and Research Branch, Islamic Azad University, Simon Bulivar Blvd, 14515/775, Tehran, Iran

[*] Corresponding author, e-mail: fadaee@srbiau.ac.ir

Received: 19 May 2022, Accepted: 19 September 2022, Published online: 08 November 2022

Abstract

Surface fault ruptures damage structures which are located at the intersecting zones of active faults. It is essential to consider the undesirable effects of surface fault ruptures when designing structures. Geotechnical measures such as reinforced soil foundations effectively mitigate the hazards related to surface faults. The present work conducted a series of tests on foundations reinforced with geosynthetics, including geogrids, geocells and geogrid-geocell layers. These tests simulated the behavior of 1.5 m-wide strip footings located in 6-m thick alluvium that had been displaced 60 cm. A total of 12 disparate tests in terms of the number and type of reinforcement were conducted at a scale factor of 10. Image analysis of the results indicated desirable behavior for reinforced soil foundations in terms of reduced angular distortion, uniform settlement and deviation of the fault path. For normal fault rupture, the angular distortion of foundations reinforced by one geogrid layer, one geocell layer, one geogrid-geocell layer or two or three geogrid layers decreased by 60%, 30%, 70%, 80% and 80%, respectively. These results also revealed that an increase in the number of geogrid layers to more than two layers caused an insignificant decrease in angular distortion. The decrease in angular distortions observed for soil foundations reinforced by one geogrid layer, one geocell layer and one geogrid-geocell layer were 7%, 16% and 40%, respectively, for reverse faulting. The performance of a reinforced soil foundation subjected to normal faulting was more acceptable than that for reverse faulting.

Keywords

geocell, geogrid, reinforced foundation, differential settlement, angular distortion, fault deviation, normal and reverse faults

1 Introduction

Differential settlement of the ground in a fault rupture zone during an earthquake will cause the ground surface to undergo surface faulting. Structures in the vicinity or on the fault surface could experience substantial damage [1]. During an earthquake, both transient seismic waves and permanent ground deformation (faulting) occur; however, most studies have emphasized the performance of structures in response to transient seismic waves [2–3]. Numerical modeling and case studies also have been carried out on the behavior of structures near fault rupture zones [4, 5].

High-magnitude earthquakes can expand fault ruptures and cause surface faulting, which can cause severe damage to structures and installations and lead to casualties [6]. Notable examples of surface faulting caused by earthquakes occurred in Kocaeli (Turkey) in 1999, Düzce (Turkey) in 1999, Chi-Chi (M = 7.6, Taiwan) in 1990 and Wenchuan (M = 7.9, China) in 2008. The Chi-Chi earthquake caused a rupture with an approximate length of 90 km and a vertical fault outcrop in some areas of approximately 10 m. In the Wenchuan earthquake, three massive parallel faults ruptured simultaneously, resulting in a surface fault with a length of 285 km. A permanent vertical offset of up to 6 m was reported in one of the lengthiest faults of this earthquake. This fault passed through several urban regions and inflicted damage to bridges, vital lines and buildings [7, 8]. Shear rupture and angular distortion are two main components affecting surface faulting [9–12].

The first recommendation of building design standards is to avoid constructing buildings near or on active faults because of the risk of fractures occurring at the ground surface during an earthquake. In most cases, the emergence of surface faulting next to or on submerged active faults cannot be precisely predicted. Thus, with increases in development in urban areas, particularly in areas with limited

Cite this article as: Ahmadi, N., Fadaee, M. "Mechanical Behavior of Soil Foundations Reinforced with Geosynthetics Exposed to Normal and Reverse Fault Ruptures", Periodica Polytechnica Civil Engineering, 67(1), pp. 123–140, 2023. https://doi.org/10.3311/PPci.20491

land and economic options, feasibility studies should be done to determine safe methods for construction of structures in active fault zones. Such studies do not prioritize avoidance of construction in active fault zones as the simplest solution. They instead investigate and propose geotechnical and structural measures to construct buildings in areas prone to surface faulting that can be controlled by engineering methods. This includes construction of linear infrastructures such as roads, expressways and tunnels that may pass over areas prone to surface faulting.

In recent decades, numerous studies have been conducted on foundation-fault rupture interaction and faulting simulation, including the use of case histories from past earthquakes [1, 6–8, 9–24], physical modeling [23, 25–29] and numerical analysis [29]. The majority of earlier studies which were concerned with geological investigation and to understand the effect of faulting of structures were carried out using sandbox models [30]. The results demonstrated that, depending on the faulting offset, surface faulting did not occur or was localized and did not reach the ground surface in cases of slight displacement. However, for large displacements, surface faulting was observed. Furthermore, footings and changes in the amount of overburden could cause deviation in the faulting path [26]. Ahmed and Bransby [31] modeled surface faulting propagation using a centrifuge with and without footings for reverse faulting. Their results suggested that the location of the footings could affect angular distortion relative to the surface faulting location.

Recently, more attention has been paid to mitigation of fault deformation. Existing mitigation strategies include strengthening of foundations, diffusion of fault deformation and deviation of the fault rupture path. The second and third strategies are geotechnical methods designed to protect structures against fault rupture. Diffusion of fault deformation requires spreading of the differential settlement to a wider zone of influence. Deviation of the fault rupture path aims to divert the fault rupture away from the foundation so that the structure remains practically unaffected by differential settlement.

Fadaee et al. [20] proposed a method to deviate the fault path from its original path with the use of a soil bentonite wall (SBW) between a structure and the faulting path. They conducted 1-g modeling to introduce a soft deformable wall barrier that could divert the fault rupture away from the structure and protect surface foundations against reverse faulting.

Studies have demonstrated the efficiency of geosynthetic reinforced soil for reducing the total and differential settlement under consolidated saturated soil, expansive soil experiencing considerable volume change over wet–dry cycles and for preserving road stability [32–37]. The primary reinforcement mechanism used has been the tensile membrane effect which refers to the use of geosynthetics and the overlaying earth to deform and absorb tensile forces to reduce the effects of ground settlement [38–40].

Bray [9] numerically studied the risk of surface faulting on geogrid-reinforced soil foundations. The results showed that a soil foundation reinforced by two or four geogrid layers reduced angular distortion of the soil at the ground surface caused by small offsets in normal faulting.

Ghalandarzadeh and Ashtiani [41] carried out centrifuge tests to study the effects of reinforcing a soil foundation with a geogrid and the use of trenches to reduce the risk of reverse faulting on surface footings. These measures included excavating vertical trenches next to footings to deviate the fault path and the use of a geogrid to expand faulting over a broader range. Their results revealed the significant effectiveness of the multiple trenches method for fault deviation. However, the geogrid layers did not significantly affect reverse faulting or the behavior of surface footings.

Moosavi et al. [42] examined the effects of geosynthetics on reducing differential displacement caused by reverse faulting using physical and numerical methods. They concluded that the use of a layer of geogrid in the soil foundation slightly reduced the magnitude of angular distortion at the ground surface.

Geosynthetics have previously been used to reduce the risk of surface faulting. One example is plans for a highway in Taiwan where a section would cross a fault where remarkable displacement had occurred along a long surface rupture during the 1999 Chi-Chi earthquake. Highway officials required that the seismic performance of this highway should be functional after a future earthquake. Experience had shown that gravity-type retaining walls were too rigid to withstand large differential settlement induced by fault displacement. The final decision of this highway extension project was, therefore, to design a ductile highway embankment to traverse the surface fault rupture zone using geosynthetic-reinforced soil (GRS) foundations instead of conventional concrete retaining walls. The GRS structure consists of a GRS wall and an underlying GRS foundation. This foundation was

adopted to improve the load bearing capacity of the foundation soil and reduce the extent of fault-induced angular distortion to an acceptable level. The GRS wall was constructed to accommodate differential settlement at the ground surface and maintain the stability and serviceability of the highway embankment [43].

The current study focused on 1-g modeling to examine the effects of geogrid, geocell and geogrid-geocell-reinforced soil foundations subjected to normal and reverse faulting on angular distortion, fault-path deviation and differential settlement. As only a limited number of studies have been conducted on normal faulting, a larger sandbox was built to allow simulation of alluvia at greater scales.

2 Test model and device

The reduced-scale model (1-g model) was tested on reinforced and unreinforced soil foundations using a sandbox. The dimensions of the sandbox were 190 × 80 × 60 cm (length × width × height). Transparent glass walls were installed in the longitudinal directions to observe and allow digital imaging of soil deformation. The bottom of the sandbox consisted of a movable hanging wall and a fixed footwall. Normal and reverse faulting was modeled by moving the hanging wall up and down by means of a hydraulic cylinder (P = 500 bar) installed beneath the hanging wall. The hydraulic jack was able to displace the soil samples vertically up to 6 cm.

The amount of offset (h) was measured using a digital ruler (LVDT) with 0.1 mm of accuracy. The distortion angle of the foundation was measured using a digital level with 0.1° of accuracy that was installed on the footing. This study investigated unreinforced foundations and those reinforced with geocells and geogrids under normal and reverse faulting conditions. The primary location of the fault tip at the sandbox roof was X = 72 cm from the left boundary. The faulting angle was set at 60°.

A sand rainer device was used to simulate the sandy soil foundation. This device produced sand foundations at a range of relative densities from loose to dense sand. The density of the sand foundations varied according to the width of the sand rainer slot/curtain (1–3 mm), the height from which the sand "rained" and the speed of raining. Fig. 1(a) shows a schematic of the sandbox and Fig. (1(b) shows an image of the sandbox and sand rainer.

The sand rainer capacity was about 500 kg. The length of the rainer curtain was equal to that of the sandbox, i.e., 80 cm. This device was used to form the traveling curtain rainer for large soil specimens.

The reinforced layers were positioned at a height of B/3 beneath the foundation, where B denotes the foundation width (15 cm in this test). At a scale factor of N = 10, the strip foundation was modeled at a width of 1.5 m. Where more than one layer was applied, the distance between layers was considered to be B/3.

3 Material characterization

3.1 Soil

This study used common Firuzkuh #161 sand (R_d = 70%) that was collected from Firuzkuh quarry in northeastern Tehran. The ASTM grain-size analysis and physical properties of the Firuzkuh sand are presented in Fig. 2 and Table 1, respectively. The F-161 sand is well sorted but poorly graded, with grains ranging in size from 0.1 to 1 mm with no evidence of clay mineral components. The mechanical strength of the sand was obtained using its internal friction angle of 32°.

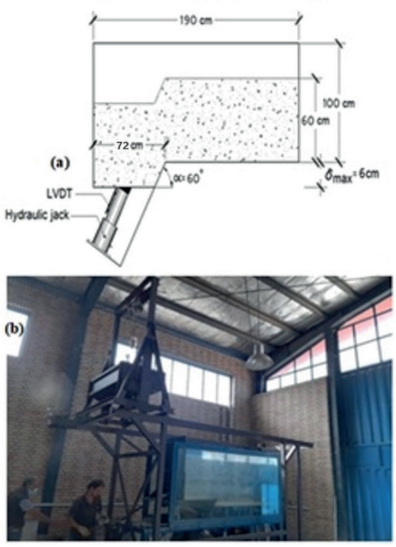

Fig. 1 (a) schematic of sandbox; (b) image of sandbox and sand rainer

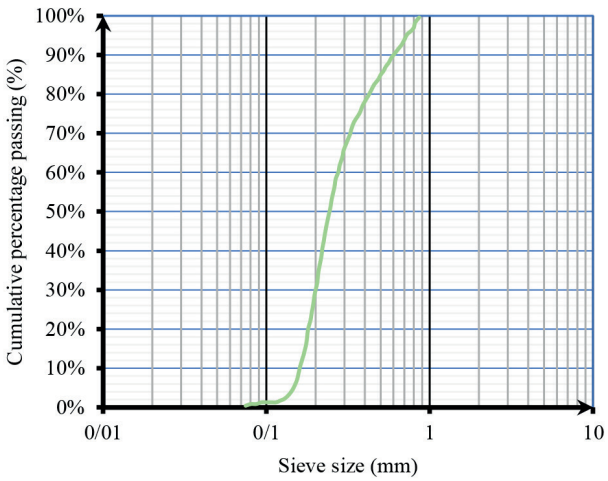

Fig. 2 Grain-size distribution curve for Firuzkuh #161 sand

Table 1 Properties of Firuzkuh #161 sand

Properties	Notation	Value
Soil type	*SP*	-
Grain density	G_s	2.61
Maximum dry unit weight	γ_{max}	1.65
Minimum dry unit weight	γ_{min}	1.37
Cohesion	*C*	0
Internal friction angle	φ	32°

Table 2 Physical and mechanical properties of geocell

Test description	Test result	Standard [44]
Tensile strength	1.29 kN/strip	ASTM D4595
Percent elongation	138.93%	ASTM D4595
Shear strength	>1.46 kN	ASTM D4595
Peel strength	0.72 kN	ASTM D4595

3.2 Reinforcements

The industrial reinforced geogrid and geocell materials used for this study were monofilament polyester and polyethylene compounds.

3.2.1 Geocell

The prototype geocell was perforated and manufactured by Energy Anasor Ayandeh (Geosakht; Iran). Table 2 demonstrates the physical and mechanical properties of geocell.

In order to select the geocell model, tensile strength testing was done of geocells composed of seven materials, five were made of isinglass and plastic and two were made of plastic floor covering. The tensile strength tests of the samples were carried out using a Geotech AI-3000 device with a velocity of 50 mm/min. After examining the results of all selected materials, one floor covering sample was selected as the geocell model because it recorded approximately one-tenth of the tensile strength relative to the prototype geocell. Fig. 3 shows a sample of the geocell used.

3.2.2 Geogrid

The geogrid used was manufactured by the Energy Anasor Ayandeh (Geosakht; Iran). It was square in shape, perforated and arranged in a two-dimensional net. Table 3 lists the characteristics of this product. The tensile strength of the geogrid was tested and the results of the final strength test and failure strain for the samples were T_{ult} = 1.5 kN/m^2 and ε_f = 15%, respectively. A geogrid with low tensile strength was used to allow observation of the simulation at scale for the 1-g model as per the scale laws in the test model. The tensile strength of the reinforcements and their hardness had to be reduced to $1/N^2$ (N = 10) for the main sample [45]. Table 3 shows the factors of scale and equivalent amounts for the geometry of the problem parameters of the original sample and model. Fig. 4 shows the mesh geogrid used in the laboratory tests.

Fig. 3 Sample geocell used in laboratory model

Table 3 Scaling factors according for simulation requirements

Parameters Geometry	Notation	Scaling factor	Simulated sample	Prototype
Foundation height	H (m)	$1/N$	0.6 m	6 m
Soil	S_p			
Target dry unit weight	γ_d	1	1.53 g/cm^3	1.53 g/cm^3
Angle of internal friction	φ	1	32°	32°
Reinforcement				
Ultimate tensile strength	T_{ult}(kN/m^2)	$1/N^2$	1.5	150
Failure strain	ε_f	1	15%	15%

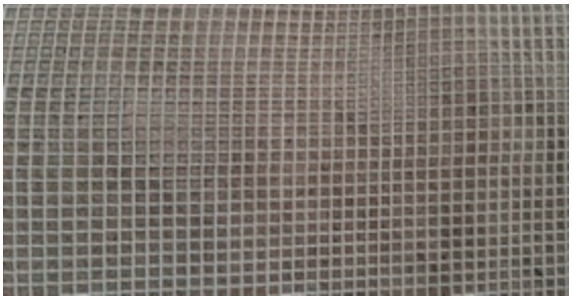

Fig. 4 Sample of geogrid used in laboratory model

4 Preparation of model and test method

Each soil layer was approximately 10 cm in thickness. A thin black sand layer was spread between each layer to delineate the change in layers. The model soil foundation was 60 cm in height and comprised fixed-density F-161 sand (R_d = 70%). Considering a scale factor of 10, a height of 60 cm is equal to a height of 6 m in the original model. During modeling the sand fall height was set at 1 m, rainer curtain width at 3 mm and rainer velocity at 0.3 m/s.

After the completion of layering, the fault was offset by the downward movement of the hanging wall at a fixed velocity. The maximum vertical offset was 6 cm. Based on the laws of simulation, the model tests simulated a vertical fault offset of up to 60 cm in the prototype. A camera was fixed in front of the box to allow observation and recording of the process of soil deformation. The geogrid, geocell or geocell-geogrid layer was placed in a specified position to prepare the reinforced foundations according to the test plan.

The data recorded by digital imaging techniques were used to obtain the soil settlement profile, angular distortion and propagation of faulting and shear failure in the reinforced and unreinforced foundations for different fault offsets. After obtaining the soil settlement profile, the angular distortion (β_{ij}) resulting from the difference in settlement was calculated using Eq. (1) as:

$$\beta_{ij} = \frac{\delta_{ij}}{l_{ij}}, \tag{1}$$

where δ_{ij} is the difference in settlement between two reference points on the footing and l_{ij} is the distance between the two reference points (Fig. 5).

The maximum angular distortion, β_{max}, is based on the maximum value of β. Considering the significant effect of angular distortion on structural performance and damage, β_{max} is regarded as a key indicator when evaluating a reinforced soil foundation [14]. A fault offset will lead to shear failure at the fault tip which then propagates up to the ground surface, resulting in apparent shear failure [9]. This is usually associated with considerable angular distortion at the ground surface.

Fault propagation inside the foundation model was observed in several high-quality images. Consecutive digital images were used to determine the settlement, displacement and angular distortion. The effect of each type of soil foundation reinforcement on β_{max} was quantified as the percentage of decrease, R_d, and can be expressed as in Eq. (2) [14].

$$R_d = \frac{\beta_{maxu} - \beta_{maxr}}{\beta_{maxu}}, \tag{2}$$

where β_{maxu} is the maximum angular distortion of the unreinforced soil foundation and β_{maxr} is the maximum angular distortion of the reinforced soil foundation.

5 Physical modeling 1-g tests

A total of 12 physical models were made on unreinforced and reinforced soil foundations. The models 1 and 2 were free-field test types for normal and reverse faulting, respectively. The models 3 and 4 were both unreinforced soil foundation types for normal and reverse faulting, respectively. The remaining eight models examined the behavior of reinforced soil foundations against normal and reverse faulting. In models 3 through 12, the center of the footing was located over the free-field outcrop point (S/B = 0.5). The testing was done under a distributed load of 0.8 kPa. Based on a scale factor of N = 10, the model simulated 8 kPa in the prototype.

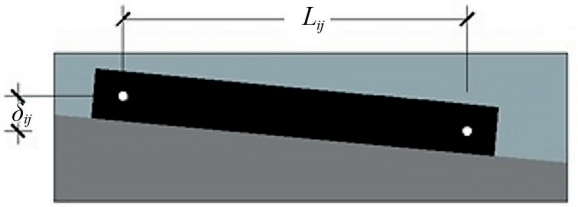

Fig. 5 Schematic of difference between base points on the foundation

5.1 Free-field foundation test for normal fault rupture (FFTNF)

The free-field foundation test was initially carried out without reinforcement to obtain the faulting outcrops at the ground surface. Fig. 6 shows the test images for normal fault rupture in the free field.

The first shear rupture (SR1) occurred at the fault tip and a distinct surface fault rupture occurred with an increase in the fault offset. The results suggest that the outcrop area was X = 93 cm from the left boundary of the box. Shear rupture propagating due to the fault offset can be observed by the relative movement of the black sand layers.

The second shear failure (SR2) occurred at h = 4 cm. It is clear that surface faulting expansion occurred as SR1 progressed in a narrow shear band. With the development of SR2, a graben was generated at the ground surface which was restricted from both sides by shearing failure of SR1 and SR2. The fault-induced influence zone was nearly 42 cm at its maximum offset of h = 6 cm. Note that the free-field faulting results are consistent with the centrifuge results [15, 22]. The field observations confirmed these results [46]. It can be seen that the maximum surface settlement at the graben occurred at the top of the normal fault tip (Fig. 6(d)). The results suggest that, with an increase in fault deformation, a narrow shear band progressed up to the fault outcrop area. The surface fault rupture was sharp and the fault outcrop location was marked on the box for comparison with later experiments.

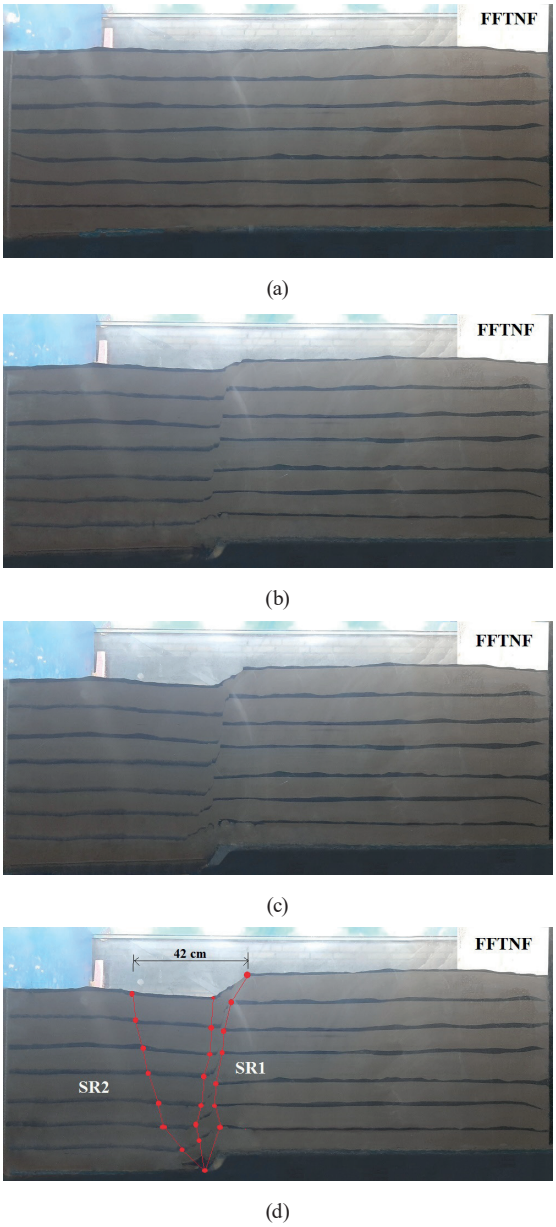

Fig. 6 Images of free-field foundation tests at different offsets: (a) $h = 0$ cm; (b) $h = 2$ cm; (c) $h = 4$ cm; (d) $h = 6$ cm

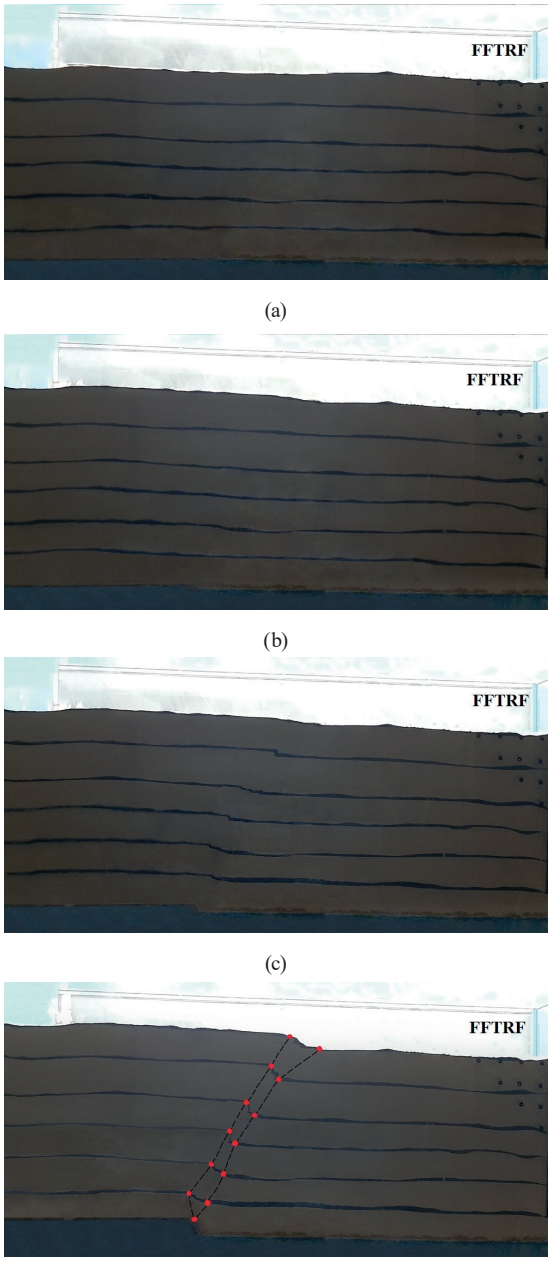

Fig. 7 Images from reverse-fault free-field foundation tests by offset value: (a) $h = 0$ cm; (b) $h = 2$ cm; (c) $h = 4$ cm; (d) $h = 6$ cm

5.2 Free-field foundation test for reverse fault rupture (FFTRF)

The free-field foundation test was performed without reinforcement to achieve fault outcrops at the ground surface. Fig. 7 shows the test images for reverse fault rupture in the free field. The shear rupture began at the fault tip, developed as the offset increased and a surface fault rupture finally appeared at the ground surface (Fig. 7(d)). The results suggest that the outcrop area is $X = 115$ cm from the left boundary of the box.

The maximum surface displacement occurred at the surface of the hanging wall (Fig. 7(d)). The test results show that, as the offset increased, a narrow shear band appeared. The surface fault rupture was sharp and the fault outcrop location was marked on the box for comparison with the experiments relating to reverse faulting. With the results of the next experiments related to reverse faulting, the width of the shear band can be compared with the results of the reverse free-field test.

5.3 Unreinforced foundation with footing and distributed load for normal fault rupture (URFNF)

Fig. 8 shows images of an unreinforced foundation with loading and a footing equivalent to that of a normal fault

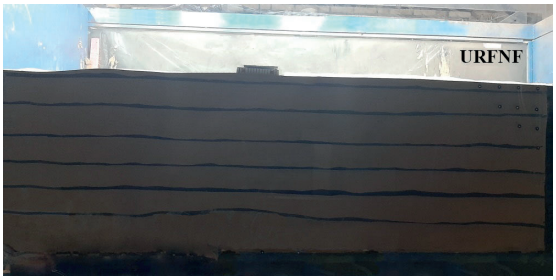

(a)

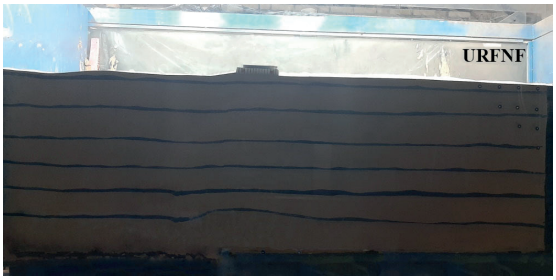

(b)

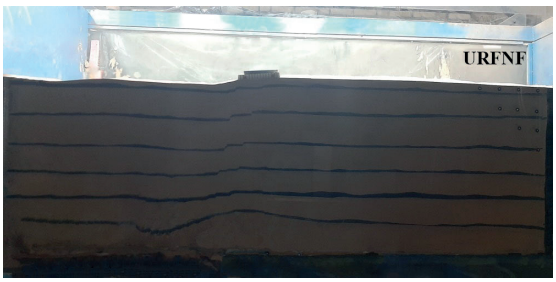

(c)

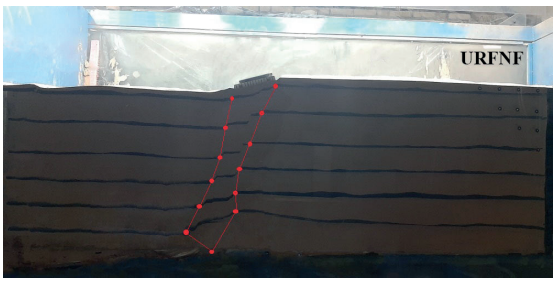

(d)

Fig. 8 Images from unreinforced foundation test with footing and overburden pressure at different fault offsets: (a) $h = 0$ cm; (b) $h = 2$ cm; (c) $h = 4$ cm; (d) $h = 6$ cm

rupture. The results show that SR1 shear failure started with an offset (h). When the results of this test are compared with those from the free-field test, more uniform settlement can be observed. The surface fault rupture was not sharp and the SR1 shear band was broader than in the free-field state, indicating the effect of the footing and distributed load on increasing the tension distribution range and shear bandwidth. Field studies indicate that the presence of overburden pressure can cause a decrease in angular distortion [26]. Thus, the existence of a footing and overburden effectively improved the behavior of the soil.

In these tests, the maximum surface settlement occurred at the top of the faulting tip and at the end of the left side of the footing, in the hanging wall. The angular distortion was measured from points i and j on the footing and the digital level points. The angular distortion (β_{max}) at the maximum vertical offset ($h = 6$ cm) was 0.33.

5.4 Unreinforced foundation with footing and distributed load for reverse fault rupture (URFRF)

Fig. 9 shows the images of an unreinforced foundation with equivalent loading and a footing under reverse fault rupture. The results indicate that shear failure initiated at the beginning of offset application and developed as the fault offset progressed.

The sharpness of the surface fault was less than that of the reverse free-field test because of the presence of the footing and the distributed load. However, the width of the shear band was narrower than in the free-field test for reverse faulting. In the layers near the footing, an increase in the width of the shear band was observed, relative to the free-field reverse faulting. The angular distortion decreased slightly.

No second shear band (SR2) was observed. The maximum surface displacement occurred at the top of the fault tip and on the left side of the footing. The maximum distortion angle (β_{max}) was 0.46 for the maximum vertical offset (6 cm). The results of this test were compared with those of the unreinforced foundations with footings and distributed loads for normal fault rupture. It was observed that the effects of distributed loading contributed less to the soil foundation behavior.

5.5 Foundation reinforced with one geogrid layer for normal fault rupture (FR1-GLNF)

One layer of geogrid having a width of four times the footing width (4B) was placed at a depth of $B/3$ beneath the footing. Fig. 10 shows the results for a foundation reinforced with one geogrid layer. It can be seen that soil settlement occurred more uniformly, especially beneath the footing and at the geogrid width (60 cm), compared to the unreinforced test.

With an increase in the fault offset for the normal fault rupture, more uniform settlement of the reinforced specimen was observed compared to the unreinforced foundation. Maximum settlement occurred at the end of the left side of the geogrid towards the hanging wall. In this situation, the zone of influence of the fault rupture equaled the geogrid width (60 cm).

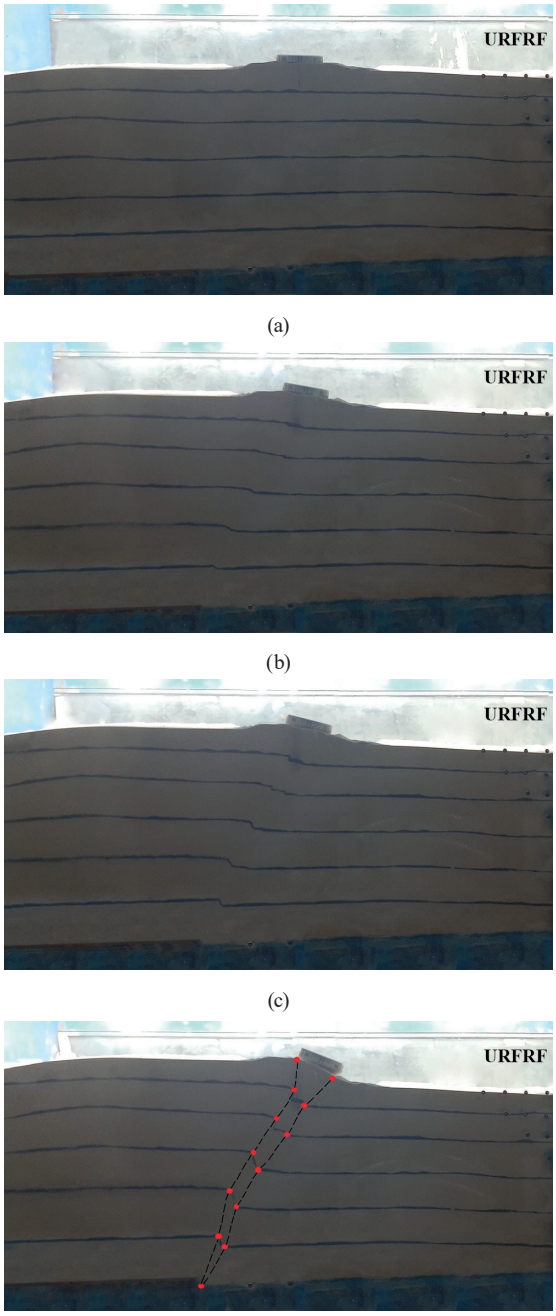

Fig. 9. Unreinforced foundation test for reverse faulting and overburden pressure at different offsets: (a) $h = 0$ cm; (b) $h = 2$ cm; (c) $h = 4$ cm; (d) $h = 6$ cm

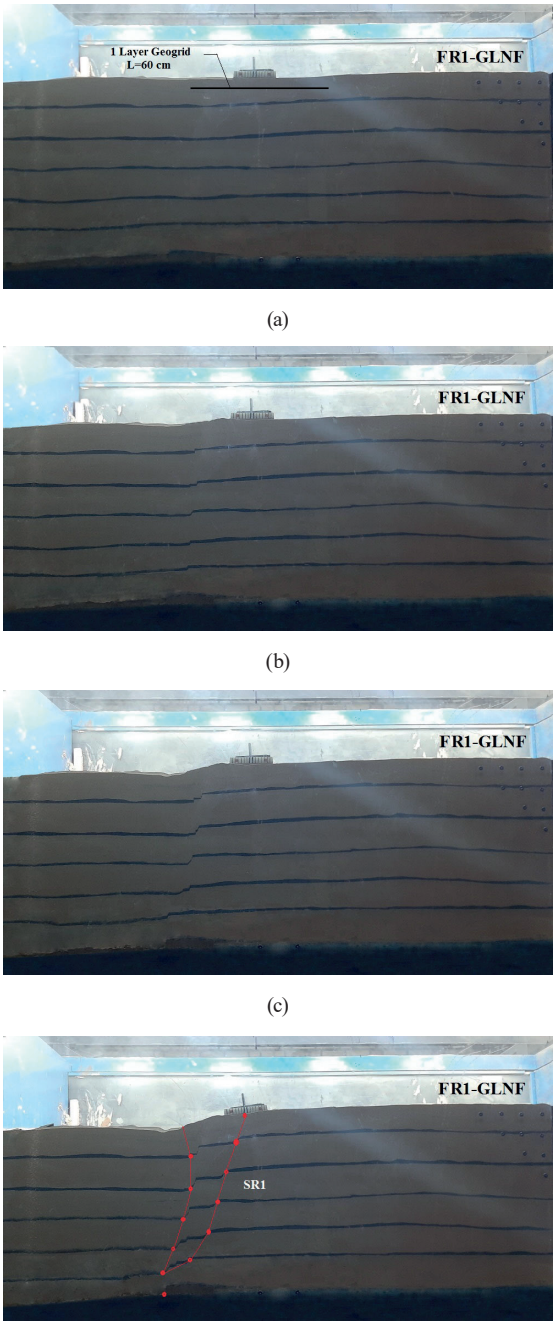

Fig. 10 Images of foundation reinforced with one layer of geogrid at different offsets: (a) $h = 0$ cm; (b) $h = 2$ cm; (c) $h = 4$ cm; (d) $h = 6$ cm

The results show that the shear band of SR1 began with an increase in the offset of the fault tip and gradually reached the ground surface (Figs. 10(a) to 10(d). However, in this condition, the surface rupture was not sharp and deviated towards the left end of the geogrid. These effects were due to the presence of a footing, distributed loading and the geogrid layer. These results are very important with regard to fault deviation from the position of the structure to protect it against fault rupture.

In this test, the shear band of SR1 was wider than for the unreinforced foundation, leading to more uniform settlement. These effects demonstrate the influence of the geogrid on the foundation performance.

Figs. 10(e) and 11 show that the right side of the shear band beneath the middle of the footing, which caused angular distortion that was far less than for unreinforced foundations. The difference in settlement of the footing separated it from the foundation at the center of the footing.

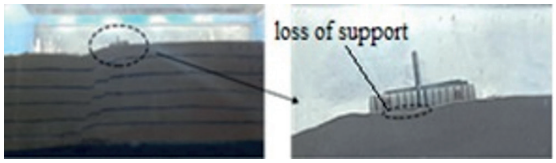

Fig. 11 Loss of support in foundation reinforced with one layer of geogrid

For this reason, deviation of faulting required more study and was investigated through testing with two and three geogrid layers. For normal faulting and a soil foundation reinforced with a geogrid layer, reinforcement was under extension. The appropriate tensile strength of geogrid was a major factor in decreasing the angular distortion of reinforced foundations. It distributed the differential settlement over a wider range which was equal to the width of the geogrid (60 cm). The maximum distortion angle (β_{max}) was 0.13 at the maximum vertical offset (6 cm). This was less than that of the unreinforced foundation.

A decrease in the angular distortion (R_d) of 60% has occurred.

5.6 Foundation reinforced with one geogrid layer in reverse fault rupture (FR1-GLRF)

Fig. 12 shows the results for a soil foundation reinforced with a geogrid layer against reverse faulting. As in the case of a soil foundation reinforced with a geogrid layer against normal faulting, a geogrid layer with a width of four times the width of the foundation (4*B*) was placed at depth *B*/3 below the foundation. The test results show that a slight decrease in angular distortion occurred compared to the unreinforced foundation and that maximum offset occurred at the left end of the footing.

There was no effect on the deviation of the fault path compared to the test for normal faulting. These results are very important with regard to fault deviation from the position of the footing or structure to protect it against fault rupture. However, the geogrid did not perform well for deviating the fault from the foundation position under reverse faulting.

The shear band was narrow, similar to that for the unreinforced soil foundation and the outline sharpness was similar to that of an unreinforced soil foundation subjected to reverse faulting.

The maximum angular distortion at a vertical offset of 6 cm (β_{max}) was 0.43 and the percentage of decrease in angular distortion was 7%. The difference in behavior of the models under normal and reverse faulting occurred because, under normal faulting, the geogrid layer was subjected to tension. The tensile strength of the geogrid layer improved the performance of the soil foundation reinforced with a geogrid for distribution of shear deformation and deviation of the fault path. However, under reverse faulting, the geogrid layer was under pressure. The very low compressive strength of the geogrid caused poor performance of the soil foundation reinforced with a geogrid layer. The results of this research confirm these results.

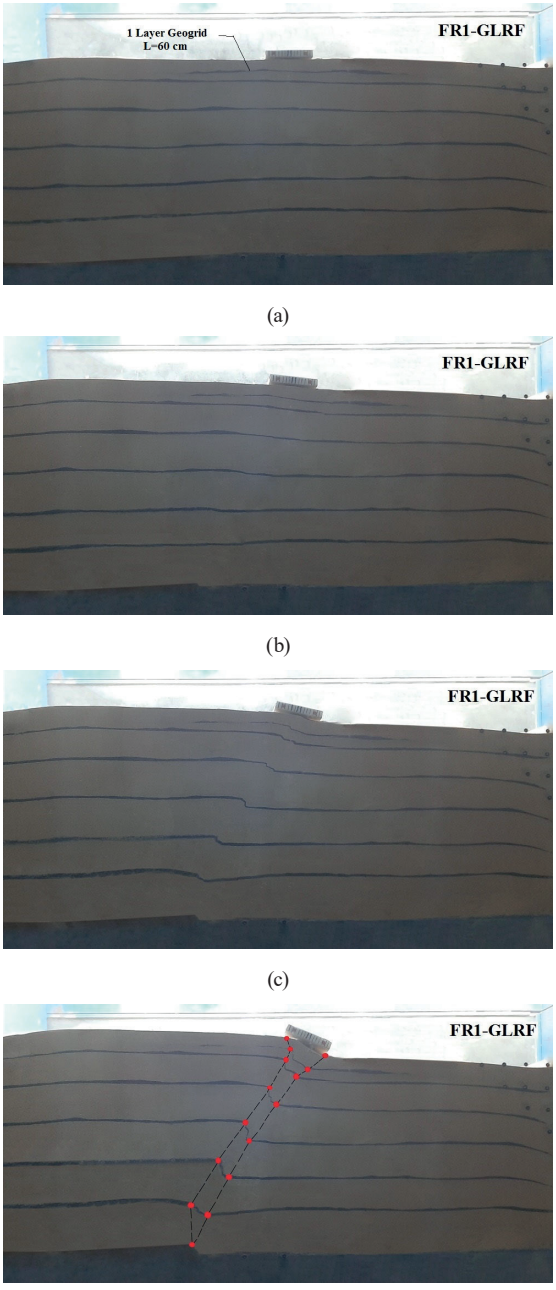

Fig. 12 Images from reverse faulting of foundation reinforced with one geogrid layer at different offsets: (a) h = 0 cm; (b) h = 2 cm; (c) h = 4 cm; (d) h = 6 cm

5.7 Foundation reinforced with one geocell layer for normal fault rupture (FR1-GLLNF)

At simulated scale, one geocell layer with a width of four times the footing width (4*B*) was placed beneath the footing at a depth of *B*/3. The geocell layer was placed in the middle of the footing at the outcrop point in the normal free-field test. Fig. 13 shows images of a soil foundation reinforced with one geocell layer. The maximum distortion angle (β_{max}) at the maximum vertical offset (6 cm) was 0.23, which was less than that for an unreinforced foundation. This indicates that a decrease in angular distortion (R_d) of 30% has occurred due to the interaction between the soil and geocell. This interaction caused spreading of the shear band in the soil above the reinforcement layer.

The fault path was similar to that of the unreinforced soil foundation. The results show that the geocell layer had a limited effect on tension distribution, expansion of the shear band and decreasing the angular distortion compared to the unreinforced soil foundation. Furthermore, the surface outcrop was not sharp due to the presence of the footing and the geocell layer. The maximum settlement occurred at the left end of the footing towards the hanging wall.

5.8 Foundation reinforced with one geocell layer in reverse fault rupture (FR1-GLLRF)

In this test, the reinforced soil foundation with one geocell layer was prepared in the same manner as that of the soil foundation reinforced with one geocell layer under the normal fault rupture test (Section 5.7). It was then exposed to reverse faulting. Figs. 14(a) to 14(d) show images of the soil foundation reinforced with one geocell layer under the effect of a reverse fault rupture.

The maximum distortion angle (β_{max}) at the maximum vertical offset (6 cm) was 0.39, which was less than that of the unreinforced foundation, indicating that a decrease in angular distortion (R_d) of 15% has occurred. The decrease in angular distortion was due to the interaction between the soil and geocell and from the compressional strength of the geocell and soil, which caused spreading of the rupture and development of a shear band.

The fault path was similar to that of the unreinforced soil foundation. The results indicate that reinforcement of the soil foundation with one geocell layer is more effective for tension distribution, expansion of the shear band and decreasing the angular distortion when compared with the soil foundation reinforced with one geogrid layer for the reverse fault rupture. The decrease in the angular distortion in the soil foundation reinforced with one geocell layer under the normal fault rupture was 30%. The surface outcrop was not sharp due to the presence of the foundation and the interaction of the geocell and soil, leading to a slight uniform outcrop relative to the unreinforced soil foundation.

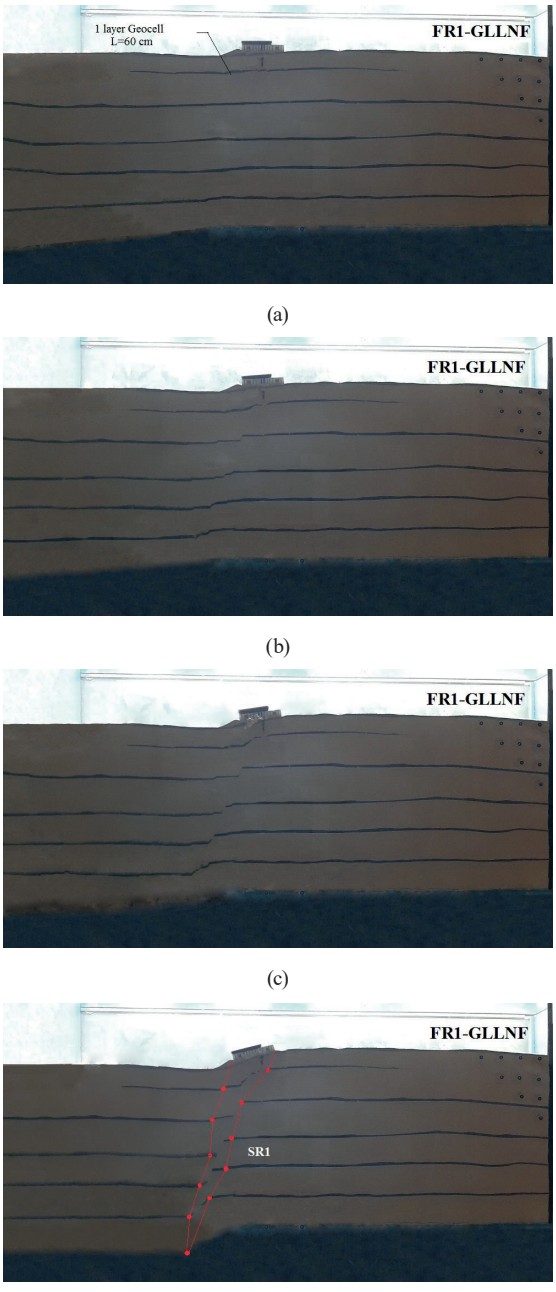

Fig. 13 Images for foundation reinforced with one geocell layer at different offsets: (a) h = 0 cm; (b) h = 2 cm; (c) h = 4 cm; (d) h = 6 cm

5.9 Foundation reinforced with one geogrid-geocell layer for normal fault rupture (FR1-GGLLNF)

In this test, one layer in which the geocell was positioned under the geogrid was used for reinforcement. The aim of combining these two layers was to obtain greater stiffness and tension resistance. This layer was located at a depth of 2B/3 beneath the footing.

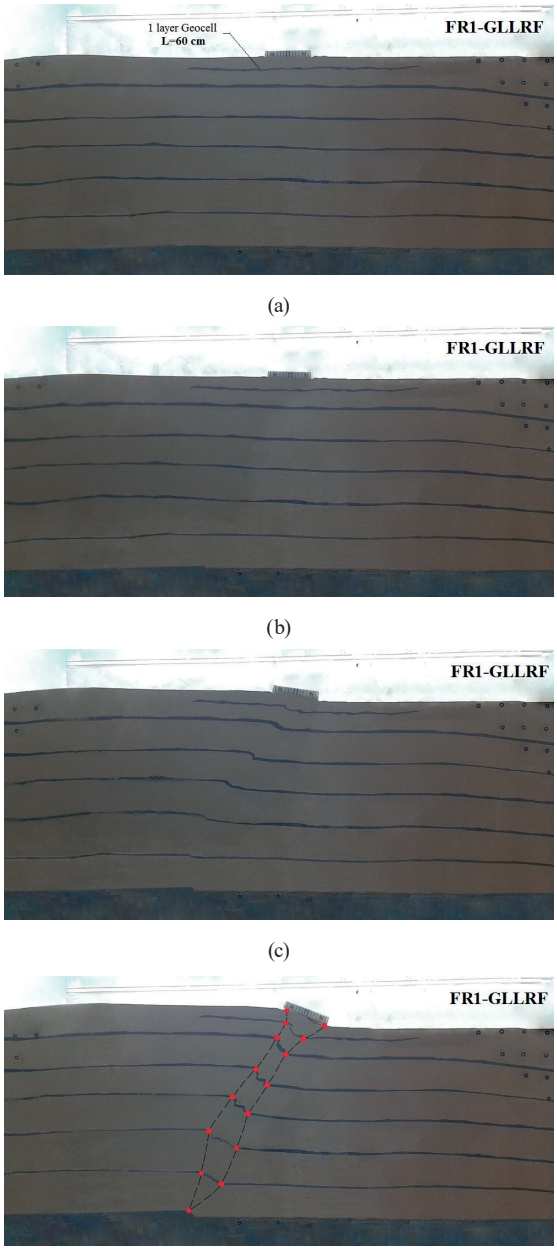

Fig. 14 Images reverse faulting foundation reinforced with one geocell layer at different offsets: (a) $h = 0$ cm; (b) $h = 2$ cm; (c) $h = 4$ cm; (d) $h = 6$ cm

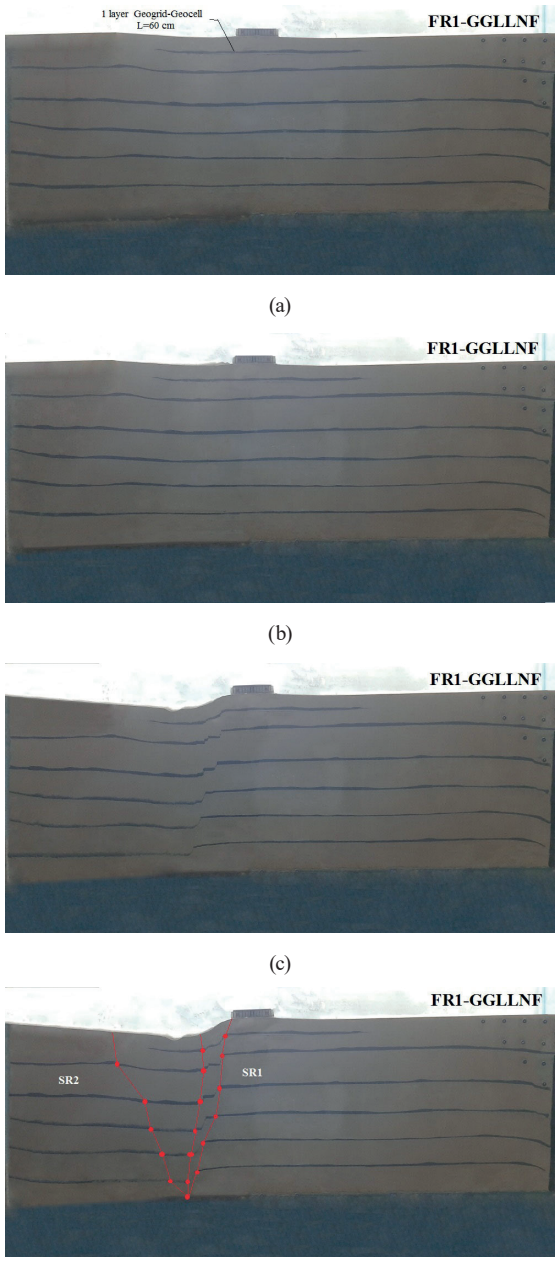

Fig. 15 Images from foundation reinforced with one geocell-geogrid layer at different offsets: (a) $h = 0$ cm; (b) $h = 2$ cm; (c) $h = 4$ cm; (d) $h = 6$ cm

Fig. 15 shows that the fault path deviated towards the left of the reinforced layer relative to the unreinforced foundation. The fault path was similar to that of the foundation reinforced with one geogrid layer. Soil settlement beneath the footing was more uniform than for the unreinforced foundation. The maximum distortion angle (β_{max}) in the maximum vertical offset (6 cm) was 0.1, which was less than for the unreinforced foundation; thus, a decrease in the angular distortion (R_d) of 70% has occurred.

When compared with the soil foundation reinforced with one geogrid layer under normal faulting, a considerable 10% decrease can be observed for angular distortion. The maximum settlement occurred at the end of the reinforcement layer towards the hanging wall. The shear band was narrower than for the foundation with one geogrid layer and it also transferred to the left side of the footing relative to the foundation reinforced with one geogrid layer.

Both shear boundaries of SR1 were located on the left side of the footing. Contrary to the performance of the one-layer geogrid, the boundary of the right side of the shear band transferred to the left side of the footing.

Foundation separation occurred with an increase in the offset on the right side of the footing, which increased the deviation of the faulting towards the left side compared to the foundation with one geogrid layer (Fig. 16). The increase in stiffness was due to the combined geocell and geogrid. The compressive strength of the geocell affected the performance of the foundation behavior reinforced with one geocell-geogrid layer.

5.10 Foundation reinforced with one geogrid-geocell layer for reverse fault rupture (FR1-GGLLRF)

The geocell-geogrid layers were placed one over the other with the geocell on top. The aim of this was to increase the stiffness and tension resistance. This combined layer was located at a depth of 2*B*/3 beneath the footing. In this case, the footing was in the middle of the reinforced layer with the midpoint of the footing on the outcrop point in the free-field test. Fig. 17 shows negligible deviation in the fault path relative to the unreinforced soil foundation under reverse faulting. The maximum distortion angle (β_{max}) at the maximum vertical offset (6 cm) was 0.27, which was less than that of the unreinforced foundation; thus, a reduction of 40% in angular distortion (R_d) has occurred.

The reduction in the angular distortion in the soil foundation reinforced with a geogrid-geocell layer under normal fault rupture was 70%. The surface outcrop was not sharp due to the presence of the foundation and the interaction of the geogrid-geocell and the soil. A slight uniform outcrop can be observed relative to the unreinforced soil foundation. The compressive strength of the geocell and the increase in stiffness resulting from the effect of the combined geogrid-geocell layer improved the behavior of the reinforced soil foundation exposed to reverse faulting.

5.11 Foundation reinforced with two geogrid layers for normal fault rupture (FR2-GLNF)

Two geogrid layers with widths of four times the footing width (4*B*) were located at depths of *B*/3 and 2*B*/3 beneath the footing. Figs. 18(a) to 18(d) show images of the foundation reinforced by two geogrid layers. It can be seen that the soil settlement was more uniform than for the unreinforced foundation and the angular distortion decreased significantly compared to the unreinforced foundation. The angular distortion was less than for the foundation reinforced with one geogrid layer. The maximum distortion angle (β_{max}) was 0.07 at the maximum vertical offset (6 cm), which is less than that of the unreinforced foundation; thus, a reduction in angular distortion (R_d) of 80% has occurred. Maximum

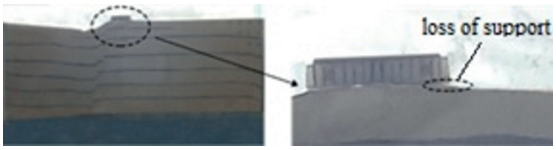

Fig. 16 Foundation reinforced with one geocell-geogrid layer

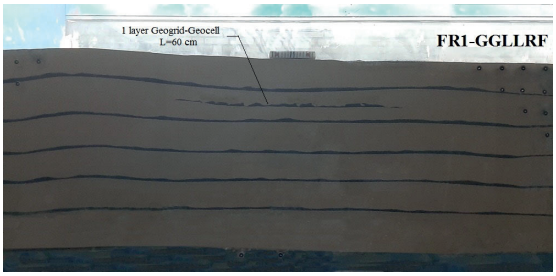

(a)

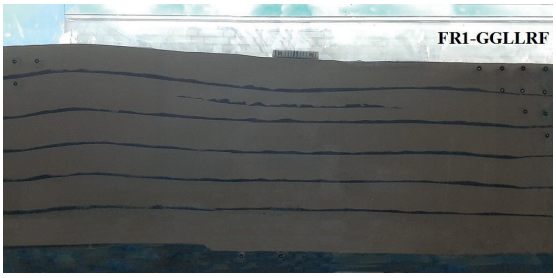

(b)

(c)

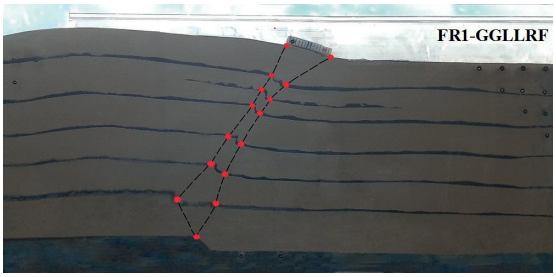

(d)

Fig. 17 Images from reverse faulting on foundation reinforced with one geocell-geogrid layer at different offsets: (a) h = 0 cm; (b) h = 2 cm; (c) h = 4 cm; (d) h = 6 cm

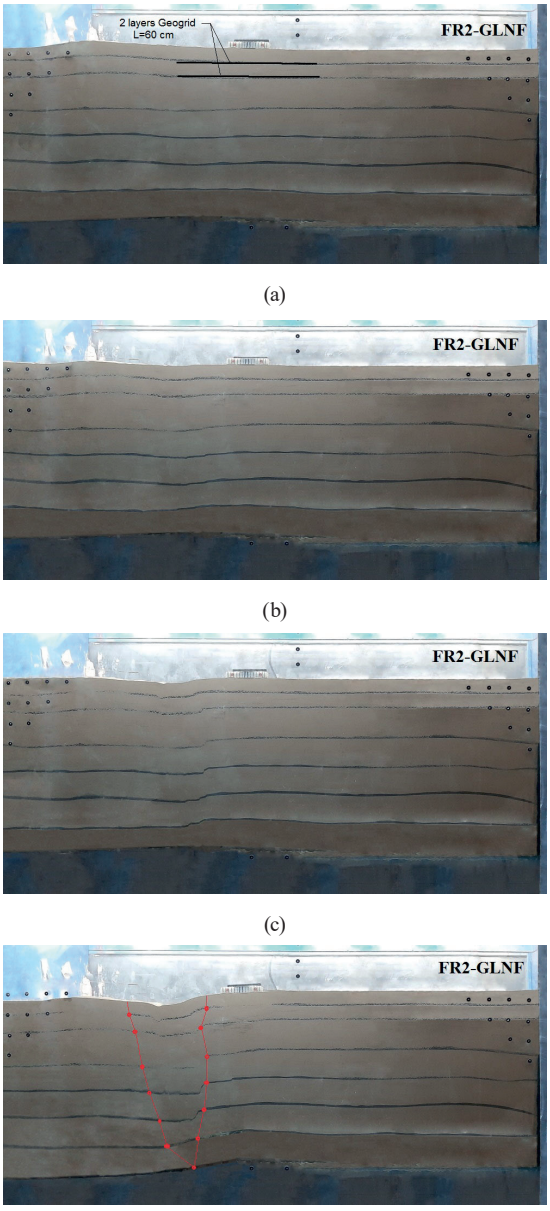

Fig. 18 Images from foundation reinforced with two geogrid layers at different offsets: (a) $h = 0$ cm; (b) $h = 1.4$ cm; (c) $h = 2.9$ cm; (d) $h = 6$ cm

settlement occurred on the left side of the reinforced layer, corresponding to the states of the geogrid-reinforced foundations where the width of all reinforcements was 4*B*. The zone of influence of the geogrid was 4*B* and the shear bandwidth increased compared to the foundation reinforced with one geogrid layer. The faulting path fully deviated towards the left side of the footing. The right boundary of the faulting shear band in the middle of the foundation reinforced with one geogrid layer transferred about 2(*B*/3) towards the left footing. This resulted in greater faulting deviation. Consequently, more uniform settlement was observed relative to the foundation reinforced with one geogrid layer.

An increase in the number of geogrid layers effectively decreased the structural damage because of the decrease in angular distortion, which caused uniform settlement and increased the broader distribution of the shear band. The fault deviated towards the left side of the footing at a point where the footing exhibited little settlement and angular distortion at the foundation footwall and soil settlement mainly transferred to the left end of the geogrid because of the fault deviation.

5.12 Foundation reinforced with three geogrid layers for normal fault rupture (FR3-GLNF)

Three geogrid layers with widths of four times the footing width (4*B*) were located at depths of *B*/3, 2(*B*/3) and *B* beneath the footing, The footing midpoint was located at the center of geogrid and the midpoints of the geogrid layers were at the outcrop point of the fault in the free-field state. Figs. 19(a) to 19(d) show images of foundations reinforced by three geogrid layers.

The results show that soil settlement occurred more uniformly relative to the previously reinforced foundations. However, the fault deviation was similar to that observed in the foundation reinforced by two geogrid layers.

The difference between this test and the foundations reinforced by one and two geogrid layers is the occurrence of outcrops on the left and right sides of the geogrid; however, the differential settlement moved toward the left side of the geogrid in this state. This caused the footing to rest completely on the foundation footwall and faulting had little effect on the performance of the foundation.

The maximum distortion angle (β_{max}) at the maximum vertical offset (6 cm) was 0.07, which was substantially less than that of the unreinforced foundation; thus, a decrease in the angular distortion (R_d) of 80% has occurred. Moreover, the fault deviation was inclined more towards the left of the footing such that it rested on the foundation footwall with almost no settlement or angular distortion. Soil settlement transferred to the left end of the geogrid with the fault deviation. Comparison with the results of foundations reinforced by two or three geogrid layers revealed that the increase to three geogrid layers had little effect on the settlement, angular distortion or fault path deviation.

Fig. 20 shows the quantitative decrease in angular distortion in the soil foundations reinforced with one geogrid layer, one geocell layer and one geocell-geogrid layer compared with that of the unreinforced soil foundation for a normal fault rupture. The results indicate that the minimum value of β_{max} occurred in the soil foundation

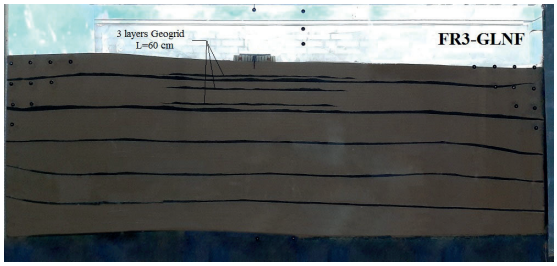

(a)

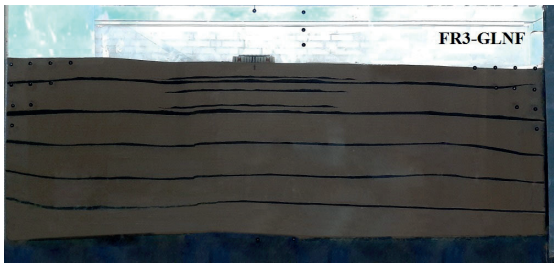

(b)

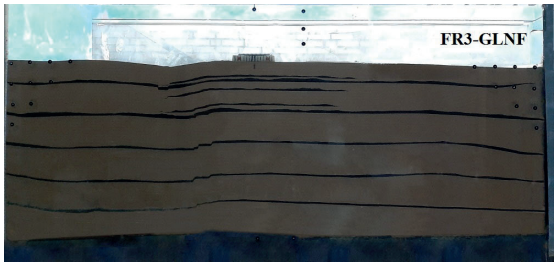

(c)

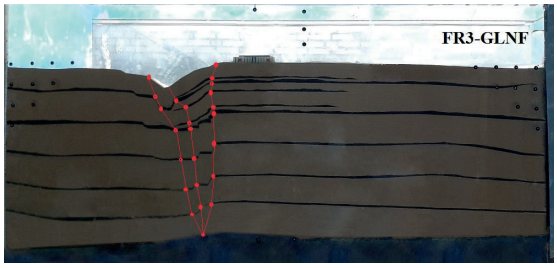

(d)

Fig. 19 Images from foundation reinforced with three geogrid layers at different offsets: (a) $h = 0$ cm; (b) $h = 1.2$ cm; (c) $h = 2.6$ cm; (d) $h = 5.2$ cm

reinforced with one geocell-geogrid layer; however, the maximum value of β_{max} was for soil foundation reinforced with one geocell layer. The acceptable behavior of soil foundation reinforced with geogrid layer against normal faulting related to the high tensile strength of the geogrid.

Fig. 21 shows a quantitative decrease in angular distortion in the soil foundations reinforced by one geogrid layer, one geocell layer and one geocell-geogrid layer compared with the performance of the unreinforced soil foundation under reverse fault rupture. The results indicate that soil foundations reinforced by the geocell-geogrid layer showed only a slight decrease in angular distortion. The minimum and maximum β_{max} values were for soil foundations reinforced by one geocell-geogrid layer and one geogrid layer, respectively. The unacceptable behavior of the soil foundation reinforced with one geogrid layer against reverse faulting was due to the low compressive strength of the geogrid layer.

Fig. 22 shows the quantitative decreases in angular distortion for the soil foundations reinforced by one, two and three geogrid layers compared to the performance of the

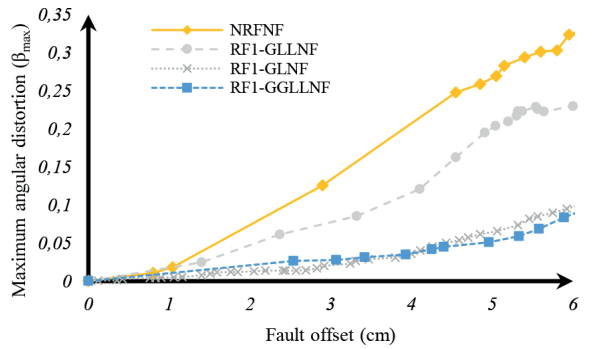

Fig. 20 Fault offset and maximum angular distortion for foundations reinforced with one geogrid layer, one geocell layer and one geogrid-geocell layer under normal faulting

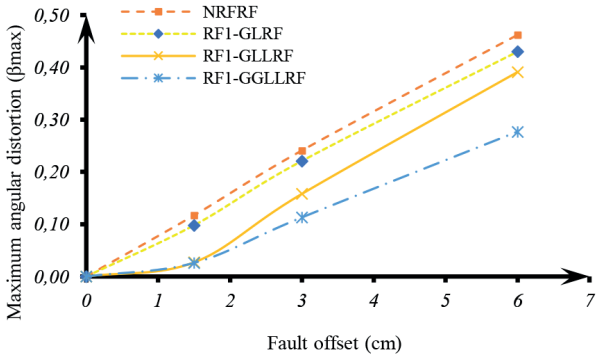

Fig. 21 Fault offset and maximum angular distortion for foundations reinforced with one geogrid layer, one geocell layer and one geogrid-geocell layer for reverse faulting

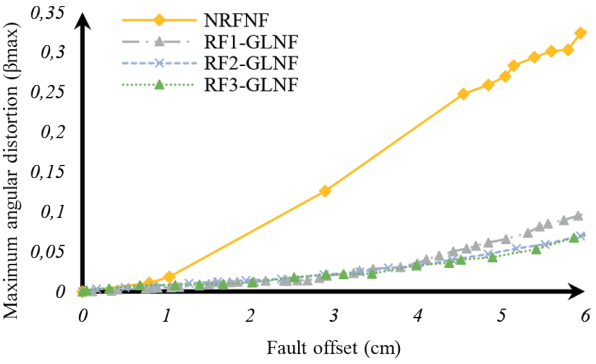

Fig. 22 Fault offset and maximum angular distortion for foundations reinforced with one, two, and three geogrid layers

unreinforced soil foundation for reverse fault rupture. The smaller β_{max} values occurred because the acceptable tensile strength of one geogrid layer increased with the use of two or three layers.

Table 4 summarizes the list of experiments and major findings obtained in this study. The major findings include the percentages of decrease in the maximum angular distortion of the reinforced soil foundations exposed to normal and reverse fault rupture.

Table 4 Test results at maximum offset (h = 6 cm) compared to unreinforced foundation

Type of test	β_{max}	R_d (%)
Free-field foundation in normal faulting	-	-
Free-field foundation in reverse faulting	-	-
Unreinforced foundation in normal fault	0.33	-
Unreinforced foundation in reverse faulting	0.46	-
Reinforced foundation with a layer of geogrid in normal faulting	0.13	60
Reinforced foundation with a layer of geogrid in reverse faulting	0.43	7
Reinforced foundation with a geocell layer in normal faulting	0.23	30
Reinforced foundation with a geocell layer in reverse faulting	0.39	15
Reinforced foundation with a geogrid-geocell layer in normal faulting	0.1	70
Reinforced foundation with a geogrid-geocell layer in reverse faulting	0.27	40
Reinforced foundation with a layer of geogrid in normal faulting	0.07	80
Reinforced foundation with a layer of geogrid in normal faulting	0.07	80

6 Conclusions

Twelve physical models were built to evaluate and compare the performance of reinforced and unreinforced soil foundations to determine the best methods of reducing the risk of surface rupture under normal and reverse faulting. The data recorded by digital imaging techniques were used to obtain the soil settlement profiles, angular distortion and fault propagation and shear failure in the reinforced and unreinforced foundations at different fault offsets.

The angular distortion at different offsets was recorded by a digital level mounted on the footing during the tests. The amount of offset corresponding to each angular distortion was recorded by an LVDT mounted on the hydraulic jack. Quantitative investigation was then carried out to examine the effect an increase the number of geogrid layers on the performance of the reinforced foundations. The main experimental results were as follows:

1. In the free field foundation test under normal faulting, the shear failure began at the fault tip with the onset of fault movement. Shear failure occurred at the ground surface with the progression of faulting. Secondary shear failure occurred on the hanging wall and resulted in a graben at the ground surface. This test was performed to obtain the fault outcrops at the ground surface. The results showed that the outcrop area was X = 93 cm from the left boundary of the box.
2. In unreinforced soil foundations, distributed loading reduced the sharpness of the surface outcrop. However, the fault rupture in this test was the same as for the free-field foundation. In this test, the midpoint of the footing was placed over the midpoint of the surface outcrop. The footing and overburden caused expansion of the shear band and the maximum angular distortion (β_{max} = 0.33) occurred at the maximum offset caused by fault rupture (h_{max} = 6 cm).
3. In the soil foundation reinforced by one geogrid layer for the normal fault mode, the geogrid layer significantly affected faulting distribution. The maximum angular distortion decreased (β_{max} = 0.13) and uniform settlement occurred. Moreover, settlement expanded over a wider area and the angular distortion decreased by 60% relative to the unreinforced foundation.
4. In a soil foundation reinforced with a geocell layer under the normal fault mode, the maximum angle of distortion decreased (β_{max} = 0.23) by about 30% relative to the unreinforced soil foundation, but the uniform settlement increased. No deviation of the faulting path relative to the unreinforced foundation was observed.
5. In the normal faulting mode, the soil foundation reinforced by one geogrid-geocell layer performed similarly to the soil foundation reinforced by one geogrid layer. The stiffness of the geocell caused the shear band to deviate further to the left of the soil foundation relative to the soil foundation reinforced by one geogrid layer. The geogrid-geocell layer reduced the maximum angular distortion (β_{max} = 0.1) by 70% relative to the unreinforced soil foundation, but the uniform settlement increased.
6. The results showed that, when two or three geogrid layers were used to reinforce a soil foundation exposed to a normal fault rupture, the maximum

angular distortion (β_{max} = 0.07) decreased by 80% relative to the unreinforced foundation. At this stage, greater deviation in the faulting path was recorded and significant uniform settlement was observed. The addition of more than two layers had no significant effect on reinforcing the foundation exposed to normal faulting.

7. In the free-field foundation test for reverse faulting, shear failure began at the fault tip at the onset of fault movement. Shear failure occurred at the ground surface with the progression of faulting. This test was performed to obtain the fault outcrops at the ground surface. The results show that the outcrop area was X = 115 cm from the left boundary of the box.
8. In unreinforced soil foundations under the reverse fault mode, the distributed load decreased the sharpness of the surface outcrop. However, the fault path was similar to that for the reverse free-field foundation path. In this test, the midpoint of the footing was placed over the midpoint of the surface outcrop. It was observed that the footing and the overburden had limited effects on increasing the shear bandwidth in the layers near the footing. The maximum angular distortion (β_{max} = 0.46) occurred at the maximum offset caused by the fault rupturing (h_{max} = 6 cm).
9. In the soil foundation reinforced by one geogrid layer in the reverse fault mode, the geogrid layer had little effect on the faulting distribution and the maximum angular distortion (β_{max} = 0.43) decreased 7% relative to the unreinforced soil foundation for reverse faulting.
10. For a soil foundation reinforced with one geocell layer for the reverse fault mode, the maximum angle of distortion (β_{max} = 0.39) decreased by about 15% relative to the unreinforced soil foundation. No deviation of the fault path relative to the unreinforced foundation was observed.

    For the soil foundation reinforced with a geocell-geogrid layer under reverse faulting, the geogrid-geocell layer caused a decrease in the maximum angular distortion (β_{max} = 0.27) of 40% relative to the unreinforced soil foundation, but the uniform settlement increased. It did not affect the deviation of the fault path.

References

[1] Argyrou, C., O'Rourke, T. D., Stewart, H. E., Wham, B. P. "Large-scale fault rupture tests on pipelines reinforced with cured-in-place linings", Journal of Geotechnical and Geoenvironmental Engineering, 145(3), 04019004, 2019. https://doi.org/10.1061/(ASCE)GT.1943-5606.0002018

[2] Kumar, P., Kumar, A., Pandey, A. D. "Spectral Characterization of Himalayan Near-Fault Ground Motion", Periodica Polytechnica Civil Engineering, 60(2), pp. 205–215, 2016. https://doi.org/10.3311/PPci.7754

[3] Soltangharaei, V., Razi, M., Gerami, M. "Comparative Evaluation of Behavior Factor of SMRF Structures for Near and Far Fault Ground Motions", Periodica Polytechnica Civil Engineering, 60(1), pp. 75–82, 2016. https://doi.org/10.3311/PPci.7625

[4] Wu, T., Chuanbo, Z., Nan, J., Yuqing, X., Zhu, B. "Study on the mechanical cumulative damage model of slope fault fracture zone under the cumulative effect of blasting vibration", Periodica Polytechnica Civil Engineering, 64(3), pp.845–858, 2020. https://doi.org/10.3311/PPci.16030

[5] Özmen, A., Sayın, E. "Seismic Response of a Historical Masonry Bridge under Near and Far-fault Ground Motions", Periodica Polytechnica Civil Engineering, 65(3), pp.946–958, 2021. https://doi.org/10.3311/PPci.17832

[6] Garcia, F. E., Bray, J. D. "Discrete element analysis of earthquake fault rupture-soil-foundation interaction", Journal of Geotechnical and Geoenvironmental Engineering, 145(9), 04019046, 2019. https://doi.org/10.1061/(ASCE)GT.1943-5606.0002092

[7] Lin, A., Ren, Z., Jia, D., Wu, X. "Co-seismic thrusting rupture and slip distribution were produced by the 2008 Mw 7.9 Wenchuan earthquake, China", Tectonophysics, 471(3–4), pp. 203–215, 2009. https://doi.org/10.1016/j.tecto.2009.02.014

[8] Yu, G., Xu, X., Klinger, Y., Diao, G., Chen, G., Feng, X., ... An, Y. "Fault-Scarp Features and Cascading-Rupture Model for the Wenchuan Earthquake (Mw7.9), Eastern Tibetan Plateau, China", Bulletin of the Seismological Society of America, 100(5B), pp. 2590–2614, 2010. https://doi.org/10.1785/0120090255

[9] Bray, J. D. "Developing mitigation measures for the hazards associated with earthquake surface fault rupture", In: Workshop on Seismic Fault Induced Failures - Possible Remedies for Damage to Urban Facilities, Tokyo, Japan, 2001, pp. 55–79.

[10] Lazarte, C. A., Bray, J. D., Johnson, A. M., Lemmer, R. E. "Surface breakage of the 1992 Landers earthquake and its effects on structures", Bulletin of the Seismological Society of America, 84(3), pp. 547–561, 1994. https://doi.org/10.1785/BSSA0840030547

[11] Anastasopoulos, I., Gazetas, G. "Foundation-structure systems over a rupturing normal fault: Part I. Observations after the Kocaeli 1999 earthquake", Bulletin of Earthquake Engineering, 5, pp. 253–275, 2007. https://doi.org/10.1007/s10518-007-9029-2

[12] Anastasopoulos, I., Gazetas, G. "Foundation-structure systems over a rupturing normal fault: Part II. Analysis of the Kocaeli case histories", Bulletin of Earthquake Engineering, 5(3), pp. 277–301, 2007. https://doi.org/10.1007/s10518-007-9030-9

[13] Faccioli, E., Anastasopoulos, I., Gazetas, G., Callerio, A., Paolucci, R. "Fault rupture–foundation interaction: selected case histories", Bulletin of Earthquake Engineering, 6, pp. 557–583, 2008. https://doi.org/10.1007/s10518-008-9089-y

[14] Yang, K.-H., Chiang, J., Lai, C.-W., Han, J., Lin, M.-L. "Performance of geosynthetic-reinforced soil foundations across a normal fault", Geotextiles and Geomembranes, 48(3), pp. 357–373, 2020. https://doi.org/10.1016/j.geotexmem.2019.12.007

[15] Anastasopoulos, I., Gazetas, G., Bransby, M. F., Davies, M. C. R., El Nahas, A. "Fault rupture propagation through sand: finite-element analysis and validation through centrifuge experiments", Journal of Geotechnical and Geoenvironmental Engineering, 133(8), pp. 943–958, 2007. https://doi.org/10.1061/(ASCE)1090-0241(2007)133:8(943)

[16] Bray, J. D., Ashmawy, A., Mukhopadhyay, G., Gath, E. M. "Use of geosynthetics to mitigate earthquake fault rupture propagation through the compacted fill", In: Proceedings of the Geosynthetics' 93 Conference, Vol. 1, Vancouver, BC, Canada, 1993, pp. 379–392.

[17] Garcia, F. E., Bray, J. D. "Discrete-element analysis of the influence of granular soil density on earthquake surface fault rupture interaction with rigid foundations", Journal of Geotechnical and Geoenvironmental Engineering, 145(11), 04019093, 2019. https://doi.org/10.1061/(ASCE)GT.1943-5606.0002163

[18] Ashtiani, M., Ghalandarzadeh, A., Mahdavi, M., Hedayati, M. "Centrifuge modeling of geotechnical mitigation measures for shallow foundations subjected to reverse faulting", Canadian Geotechnical Journal, 55(8), pp. 1130–1143, 2018. https://doi.org/10.1139/cgj-2017-0093

[19] Loli, M., Kourkoulis, R., Gazetas, G. "Physical and numerical modeling of hybrid foundations to mitigate seismic fault rupture effects", Journal of Geotechnical and Geoenvironmental Engineering, 144(11), 04018083, 2018. https://doi.org/10.1061/(ASCE)GT.1943-5606.0001966

[20] Fadaee, M., Ezzatyazdi, P., Anastasopoulos, I., Gazetas, G. "Mitigation of reverse faulting deformation using a soil bentonite wall: Dimensional analysis, parametric study, design implications", Soil Dynamics and Earthquake Engineering, 89, pp. 248–261, 2016. https://doi.org/10.1016/j.soildyn.2016.04.007

[21] Oettle, N. K., Bray, J. D. "Geotechnical mitigation strategies for earthquake surface fault rupture", Journal of Geotechnical and Geoenvironmental Engineering, 139(11), pp. 1864–1874, 2013. https://doi.org/10.1061/(ASCE)GT.1943-5606.0000933

[22] Anastasopoulos, I., Gazetas, G., Bransby, M. F., Davies, M. C. R., El Nahas, A. "Normal fault rupture interaction with strip foundations", Journal of Geotechnical and Geoenvironmental Engineering, 135(3), pp. 359–370, 2009. https://doi.org/10.1061/(ASCE)1090-0241(2009)135:3(359)

[23] Moosavi, S. M., Jafari, M. K. "Investigation of the surface fault rupture hazard mitigation by geosynthetics", In: Proceedings of the 15th World Conference on Earthquake Engineering, Lisbon, Portugal, 2012, pp. 9354–9362. ISBN: 978-1-63439-651-6

[24] Ulusay, R., Aydan, Ö., Hamada, M. "The behavior of structures built on active fault zones: examples from the recent earthquakes of Turkey", Structural Engineering/Earthquake Engineering, 19(2), pp. 149s–167s, 2002. https://doi.org/10.2208/jsceseee.19.149s

[25] Lee, J. W., Hamada, M. "An experimental study on earthquake fault rupture propagation through a sandy soil deposit", Structural Engineering/Earthquake Engineering, 22(1), pp. 1s–13s, 2005. https://doi.org/10.2208/jsceseee.22.1s

[26] Bransby, M. F., Davies, M. C. R., Nahas, A. E. "Centrifuge modeling of normal fault-foundation interaction", Bulletin of Earthquake Engineering, 6, pp. 585–605, 2008. https://doi.org/10.1007/s10518-008-9079-0

[27] Bransby, M. F., Davies, M. C. R., El Nahas, A., Nagaoka, S. "Centrifuge modeling of reverse fault-foundation interaction", Bulletin of Earthquake Engineering, 6, pp. 607–628, 2008. https://doi.org/10.1007/s10518-008-9080-7

[28] Lade, P. V., Cole Jr, D. A., Cummings, D. "Multiple failures surface over dip-slip faults", Journal of Geotechnical Engineering, 110(5), pp. 616–627, 1984. https://doi.org/10.1061/(ASCE)0733-9410(1984)110:5(616)

[29] Lin, M.-L., Chung, C.-F., Jeng, F.-S., Yao, T.-C. "The deformation of overburdened soil induced by thrust faulting and its impact on underground tunnels", Engineering Geology, 92, pp. 110–132, 2007. https://doi.org/10.1016/j.enggeo.2007.03.008

[30] Bray, J. D. "The effects of tectonic movements on stresses and deformations in earth embankments", Doctoral dissertation, University of California, 1990.

[31] Ahmed, W., Bransby, M. F. "Interaction of shallow foundations with reverse faults", Journal of Geotechnical and Geoenvironmental Engineering, 135(7), pp. 914–924, 2009. https://doi.org/10.1061/(ASCE)GT.1943-5606.0000072

[32] Ardah, A., Abu-Farsakh, M. Y., Voyiadjis, G. Z. "Numerical evaluation of the effect of the differential settlement on the performance of GRS-IBS", Geosynthetics International, 25(4), pp. 427–441, 2018. https://doi.org/10.1680/jgein.18.00026

[33] Sadat, M. R., Huang, J., Bin-Shafique, S., Rezaeimalek, S. "Study of the behavior of mechanically stabilized earth (MSE) walls subjected to differential settlements", Geotextiles and Geomembranes, 46(1), pp. 77–90, 2018. https://doi.org/10.1016/j.geotexmem.2017.10.006

[34] Huang, C.-C. "Failure mechanisms of steep-faced geosynthetic-reinforced retaining walls subjected to toe scouring", Marine Georesources & Geotechnology, 35(8), pp. 1099–1110, 2017. https://doi.org/10.1080/1064119X.2017.1290170

[35] Talebi, M., Meehan, C. L., Leshchinsky, D. "Applied bearing pressure beneath a reinforced soil foundation used in a geosynthetic reinforced soil integrated bridge system", Geotextiles and Geomembranes, 45(6), pp. 580–591, 2017. https://doi.org/10.1016/j.geotexmem.2017.07.008

[36] Chen, J.-F., Tolooiyan, A., Xue, J.-F., Shi, Z.-M. "Performance of a geogrid reinforced soil wall on PVD drained multilayer soft soils", Geotextiles and Geomembranes, 44(3), pp. 219–229, 2016. https://doi.org/10.1016/j.geotexmem.2015.10.001

[37] Kost, A. D., Filz, G. M., Cousins, T., Brown, M. C. "Full-Scale Investigation of Differential Settlements beneath a GRS Bridge Abutment: An Overview", In: Geo-Congress 2014: Geo-characterization and Modeling for Sustainability, Atlanta, GA, USA, 2014, pp. 4203-4212. ISBN: 9780784413272 https://doi.org/10.1061/9780784413272.408

[38] King, L., Bouazza, A., Gaudin, C., O'Loughlin, C. D., Bui, H. H. "The behavior of geosynthetic-reinforced piled embankments with defective piles", Journal of Geotechnical and Geoenvironmental Engineering, 145(11), 04019090, 2019. https://doi.org/10.1061/(ASCE)GT.1943-5606.0002125

[39] Holz, R. D., Christopher, B. R., Berg, R. R. "Geosynthetic design and construction guidelines", Federal Highway Administration, Washington, DC, USA, No. FHWA HI-95-038, 1998.

[40] Giroud, J. P., Bonaparte, R., Beech, J. F., Gross, B. A. "Design of soil layer-geosynthetic systems overlying voids", Geotextiles and Geomembranes, 9(1), pp. 11–50, 1990. https://doi.org/10.1016/0266-1144(90)90004-V

[41] Ghalandarzadeh, A., Ashtiani, M. "Geotechnical mitigation measures for the interaction of reverse faulting and shallow foundations: centrifuge modeling", In: The 19th International Conference on Soil Mechanics and Geotechnical Engineering, Seoul, South Korea, 2017.

[42] Moosavi, S. M., Jafari, M. K., Kamalian, M., Shafiei, A. "Experimental investigation of reverse fault rupture-rigid shallow foundation interaction", International Journal of Civil Engineering, 8(2), pp. 85–98, 2010.

[43] Chen, Y.-G., Chen, W.-S., Lee, J.-C., Lee, Y.-H., Lee, C.-T., Chang, H.-C., Lo, C.-H. "Surface rupture of the 1999 Chi-Chi earthquake yields insights into the active tectonics of central Taiwan", Bulletin of the Seismological Society of America, 91(5), pp. 977–985, 2001. https://doi.org/10.1785/0120000721

[44] ASTM "ASTM D4595 Standard Test Method for Tensile Properties of Geotextiles by the Wide-Width Strip Method", ASTM International, West Conshohocken, PA, USA, 2017. https://doi.org/10.1520/D4595-17

[45] Viswanadham, B. V. S., König, D. "Studies on scaling and instrumentation of a geogrid", Geotextiles and Geomembranes, 22(5), pp. 307–328, 2004. https://doi.org/10.1016/S0266-1144(03)00045-1

[46] Bray, J. D., Seed, R. B., Cluff, L. S., Seed, H. B. "Earthquake fault rupture propagation through the soil", Journal of Geotechnical Engineering, 120(3), pp. 543–561, 1994. https://doi.org/10.1061/(ASCE)0733-9410(1994)120:3(543)